New results from the PHOBOS experiment

G. Roland[a] (for the PHOBOS* Collaboration)

[a]Massachusetts Institute of Technology, Cambridge, MA 02139-4307, USA

Over the past five years, PHOBOS has collected data on p+p, d+Au, Au+Au and Cu+Cu collisions, covering a wide range of collision energy, collision centrality and system size. Using these data, we have identified scaling features that are common for all types of high-energy collisions, as well as collective effects that are unique to the conditions created in collisions of relativistic nuclei. In this paper, we will focus on recent results obtained for collisions of Cu nuclei. Both in terms of universal features of particle production, and in the development of truly collective effects, the results for Cu nuclei confirm and extend our present understanding of nuclear collisions at the highest energies. In addition, we will describe recent unique results on multiplicity fluctuations and particle production at very low transverse momenta.

1. OVERVIEW

PHOBOS is one of four experiments at the Relativistic Heavy Ion Collider (RHIC) at Brookhaven National Lab, studying collisions of heavy nuclei at energies up to $\sqrt{s_{NN}} =$ 200 GeV. Our goal is to study the properties of strongly interacting matter at extreme temperature and density, where ab initio numerical QCD calculations predict a phase transition to a system dominated by quark and gluon degrees of freedom. Our findings from the first four years of these studies have been summarized in [1]. There we argued that in Au+Au collisions, a dense, highly interacting system is created, with energy densities far in excess of the critical values for the QCD phase transition.

2. THE PHOBOS EXPERIMENT

A detailed description of the PHOBOS detector can be found in [2]. The main components of the apparatus are a two-arm high-resolution magnetic spectrometer near mid-rapidity and a nearly 4π charged particle multiplicity detector covering $|\eta| < 5.4$. Both the spectrometer and multiplicity array use analog readout silicon pad sensors for particle detection, with a total of 135000 channels. The silicon detectors are complemented by scintillator based trigger and time-of-flight counters, and forward calorimeters used for event characterization by detecting spectator nucleons. In five runs at RHIC, PHOBOS has collected more than 10^9 events to tape. An overview of the available datasets can be found in Table 1. A key component of the experiment that is not usually discussed is the unique offline computing architecture that PHOBOS has established at the RHIC

*For the full list of PHOBOS authors and acknowledgements, see appendix 'Collaborations' of this volume

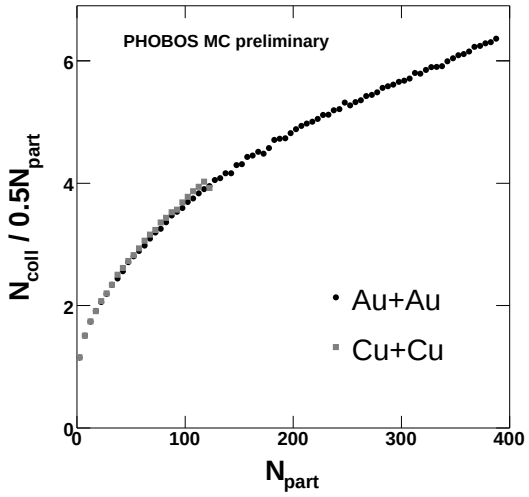

Figure 1. Ratio of the average number of collisions per participant, $\bar{\nu}$, for Cu+Cu (light symbols) and Au+Au (dark symbols) as a function of N_{part} for $\sqrt{s_{NN}} = 200$ GeV from the PHOBOS Glauber MC.

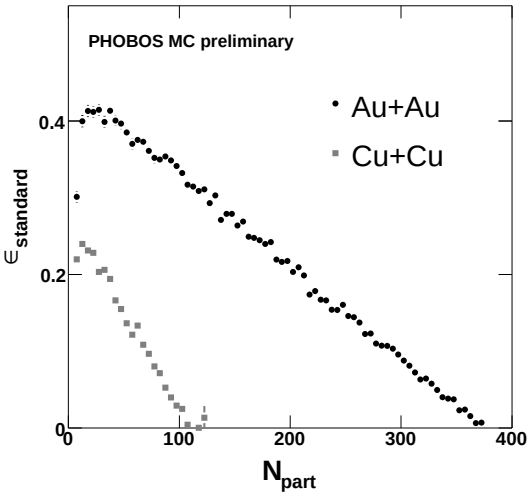

Figure 2. Average eccentricity, ϵ_{std}, of the collision zone in Cu+Cu (light symbols) and Au+Au (dark symbols) as a function of N_{part} for $\sqrt{s_{NN}} = 200$ GeV from the PHOBOS Glauber MC.

computing facility (RCF). We decided at an early stage to implement a distributed disk solution, equipping all nodes in our RCF Linux farm with cheap disk drives, for a total storage capacity of close to 100 TByte. That allows us to keep our entire physics dataset available on disk for analysis at all times. In addition, we developed effective data management software and collaborated in the development of the PROOF extensions of ROOT [3], allowing us to use the main RCF cluster for interactive, parallel analysis of the large Cu+Cu and Au+Au data samples. The effective bandwidth achieved in these analyses using PROOF at RCF exceeds 5 GByte/sec. Details of the PHOBOS computing architecture can be found in [4] and a forthcoming publication.

	p+p	**d+Au**	**Cu+Cu**	**Au+Au**
410 GeV	20			
200 GeV	100	150	400	250
130 GeV			110	4.3
62.4 GeV				22
55.9 GeV				1.8
22.5 GeV			20	
19.6 GeV				~ 1

Table 1
Number of events stored to tape in millions for different systems from p+p to Au+Au and different collision energies $\sqrt{s_{NN}}$.

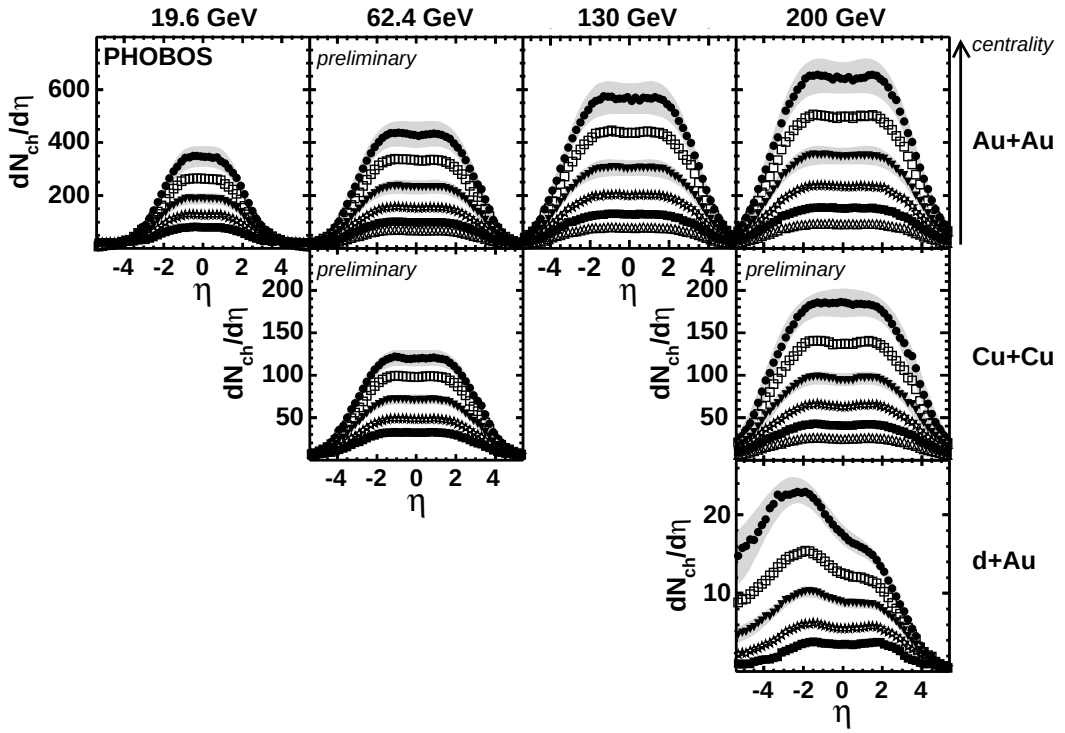

Figure 3. Charged hadron pseudorapidity distributions for different centralities for Au+Au collisions at $\sqrt{s_{NN}} =$ 19.6, 62.4, 130 and 200 GeV (top row from left to right), Cu+Cu at 62.4 and 200 GeV (middle row, preliminary) and d+Au at 200 GeV (bottom row).

3. PHYSICS RESULTS

From the very beginning, the goal of PHOBOS was to obtain a broad survey of particle production in nuclear collisions for a large variety of system size, collision centralities and collision energies. As Table 1 shows, we have indeed collected the datasets to fulfill this original program. Using these data, we attempt to extract organizing principles or scaling features directly from a systematic study of the available observables. As we will show in the following, several striking scaling rules have indeed emerged from the data. Some of those appear to connect the results obtained in nucleus-nucleus collisions with those in more elementary collisions, like p+p, p+A or e^+e^-. Other results show the existence of unique collective effects not present in elementary systems. Clearly, the true significance of these features will be established when they can be shown to naturally emerge from the eventual theoretical understanding of the physics of these collisions, or when future experiments at much higher energy at the LHC can be shown to be constrained by the same underlying features as data at present energies.

In the following subsections, we will use the PHOBOS data to address three distinct questions about scaling of particle multiplicities and distributions in nucleus-nucleus collisions. The first question concerns the scaling of overall particle production in Cu+Cu

and Au+Au collisions. Next we will investigate the connection between the centrality and energy dependence of particle production and finally we will study the connection between of the final-state azimuthal anisotropy and the initial state geometry.

As we will show in the following, conclusive answers emerge from the data for all these questions. It is important however to consider what differences between Au+Au and Cu+Cu could be expected based on the underlying differences in collision geometry. For this, the result of our Glauber calculations plotted in Figs. 1 and 2 are important. Shown in Fig. 1 is $\bar{\nu}$, the average number of binary NN collisions every nucleon undergoes within a nucleus-nucleus collision, as a function of the number of participating nucleons N_{part}. As this plot shows, a study of the centrality dependence of particle production allows a large variation of $\bar{\nu}$. However, for a given value of N_{part}, $\bar{\nu}$ in Cu+Cu and Au+Au is the same within the possible experimental resolution and therefore the Cu+Cu vs. Au+Au comparison does not provide additional discriminating power for distinguishing N_{coll} vs. N_{part} scaling. To better discriminate effects scaling with the number of binary collisions N_{coll} from those scaling with N_{part}, a comparison of Au+Au results with those from much smaller nuclei like e.g. silicon or carbon would be necessary. However, Fig. 2 shows that there is a very important difference between the collision geometry in Cu+Cu and Au+Au, even at the same N_{part}. In this figure, the average eccentricity, ϵ_{std}, of the collision zone in the transverse plane is plotted against N_{part}. Naturally, for the same N_{part} the eccentricity in peripheral Au+Au collisions is much larger than in the corresponding more central Cu+Cu collisions. The comparison of Cu+Cu and Au+Au will therefore allow a direct investigation of the connection between initial density and the efficiency with which the collision system translates the initial state geometrical asymmetry, characterized by ϵ_{std}, into a final state asymmetry in the momemtum distributions. The results of this comparison, which require a detailed understanding of the definition of the appropriate eccentricity measure, will be discussed in detail in section 3.3.

3.1. System-size dependence of particle production

One of the main questions for the Cu+Cu run at RHIC in early 2005 was that of the system-size dependence of particle production in nuclear collision at RHIC energies, in terms of overall multiplicity, $dN/d\eta$ distributions and dN/dp_T distributions. Before discussing in detail some of the scaling features observed in the data, Fig. 3 gives an impression of the breadth and quality of the data collected by PHOBOS. The figure shows charged hadron pseudorapidity distributions as a function of centrality for Au+Au collisions at $\sqrt{s_{_{NN}}} =$ 19.6, 62.4, 130 and 200 GeV [5,6], Cu+Cu at 62.4 and 200 GeV and d+Au at 200 GeV [7].

For both Au+Au and Cu+Cu collisions, the centrality selection was based on the distribution of energy deposited in the region of the multiplicity counter covering $|\eta| < 3.0$ and in the trigger counters covering $3.2 < |\eta| < 4.5$. The energy distributions for a minimum bias dataset are divided into bins of fractional cross-section and the average number of participants for each bin is determined from a Glauber calculation using the HIJING event generator [8] and a GEANT-based simulation of the PHOBOS detector response. Details of this method can be found in [1].

For the comparison of $dN/d\eta$ distributions in Cu+Cu and Au+Au, we selected centrality bins in Cu+Cu and Au+Au such that the average number of participants approx-

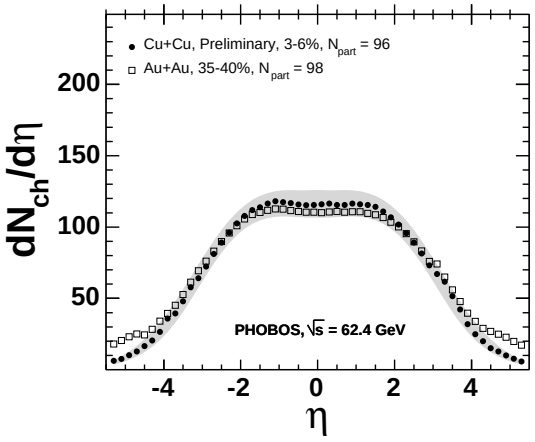

Figure 4. Pseudorapidity distribution for charged hadrons in Cu+Cu collisions (black symbols) and Au+Au collisions (open symbols) at $\sqrt{s_{NN}}$ = 62.4 GeV. The Cu+Cu and Au+Au centralities were selected to yield similar N_{part}. The grey band indicates the systematic uncertainty for Cu+Cu (90% C.L.). Errors for Au+Au are not shown.

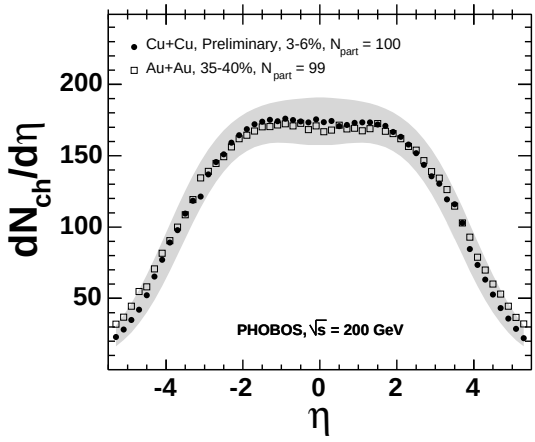

Figure 5. Pseudorapidity distribution for charged hadrons in Cu+Cu collisions (black symbols) and Au+Au collisions (open symbols) at $\sqrt{s_{NN}}$ = 200 GeV. The Cu+Cu and Au+Au centralities were selected to yield similar N_{part}. The grey band indicates the systematic uncertainty for Cu+Cu (90% C.L.). Errors for Au+Au are not shown.

imately matched. The result of this comparison is shown in Figs. 4 and 5 for collisions at 62.4 GeV and 200 GeV, respectively. No further scaling factors are applied. This comparison, and further studies for different centrality bins, provide a strikingly simple answer to the question above: If Cu+Cu and Au+Au collisions at the same collision energy are selected to have the same $\langle N_{part} \rangle$, the resulting charged particle $dN/d\eta$ distributions are nearly identical, both in the mid-rapidity particle density and the width of the distribution. This is true for both 62.4 GeV and 200 GeV data.

Following the similarity in both the mid-rapidity density and the shape of the pseudorapidity distribution, it is natural to compare particle production as a function of transverse momentum in Cu+Cu and Au+Au, for different centrality classes. This comparison can be seen in Fig.6, where we plot the nuclear modification factor R_{AA} as a function of N_{part} for Cu+Cu and Au+Au collisions at 200 GeV, in bins of p_T from 0.25 to 6.25 GeV/c. R_{AA} is defined as

$$R_{AA}(p_T) = \frac{\sigma_{pp}^{inel}}{\langle N_{coll} \rangle} \frac{d^2 N_{AA}/dp_T d\eta}{d^2 \sigma_{pp}/dp_T d\eta}. \quad (1)$$

For Au+Au, data from PHOBOS [9] and PHENIX [10] are shown. It is important to note again that the same N_{part} value in Cu+Cu and Au+Au corresponds to virtually the same value of N_{coll} for both systems. Therefore, the fact that R_{AA} coincides for Cu+Cu and Au+Au at the same N_{part}, as shown in Fig. 6 implies that for a given system size, measured by either N_{part} or N_{coll}, the absolute yield per participant is the same in

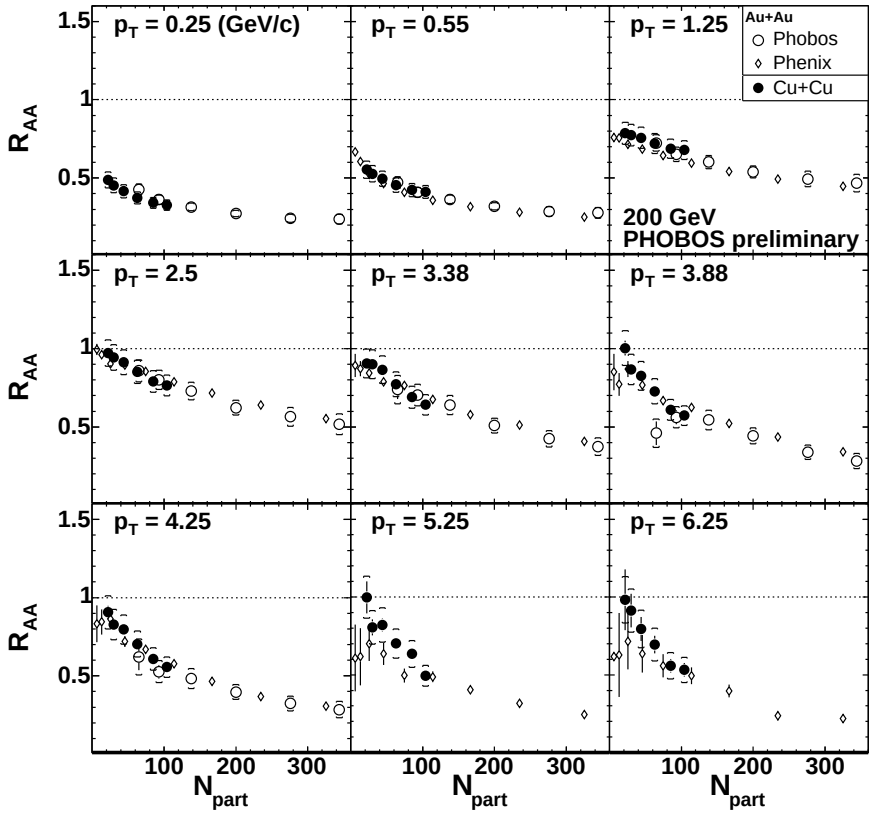

Figure 6. Nuclear modification factor R_{AA} as a function of N_{part} in bins of p_T for collisions at$\sqrt{s_{NN}}$ = 200 GeV near mid-rapdity. Data for Cu+Cu collisions (filled symbols) are shown in comparison with data for Au+Au collisions from PHOBOS (open circles) and PHENIX (open diamonds). Systematic errors for Cu+Cu data (90% C.L.) are shown as brackets.

both systems. This statement holds over the entire range in centrality and p_T covered in this analysis and is also confirmed with similar precision in collisions at 62.4 GeV. In summary, overall particle production per participant, as well as particle distribution in pseudorapidity and transverse momentum, appear identical in Cu+Cu and Au+Au at a given collision energy, if collisions with the same average number of participants are selected.

3.2. Factorization of energy and centrality dependence

While the comparison of particle production in Cu+Cu and Au+Au at the same collision energy yields the simplest possible connection between the two systems, a simultaneous study of centrality and energy dependence of the same observables for either of the systems yields a subtle and surprising scaling relationship, that again holds for mid-rapidity particle production, the shape of the $dN/d\eta$ distributions and the transverse momentum distributions. As was first shown for the mid-rapidity density [11], the ob-

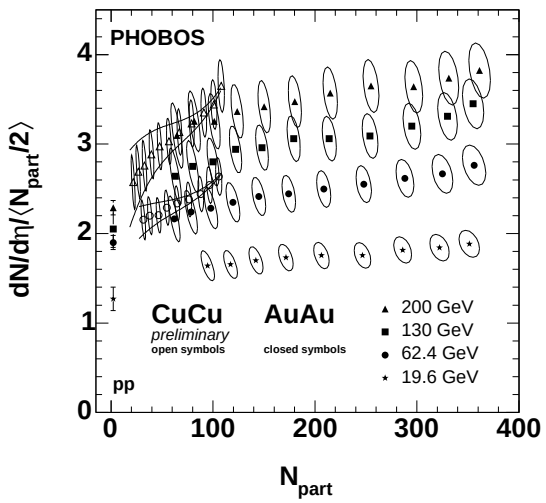

Figure 7. Mid-rapidity density $dN/d\eta/\langle N_{part}/2\rangle$ as a function of N_{part}. Au+Au data for $\sqrt{s_{NN}}$ = 19.6, 62.4, 130 and 200 GeV are shown as filled symbols, Cu+Cu data for $\sqrt{s_{NN}}$ = 62.4, and 200 GeV are shown as open symbols. Ellipses indicate the uncertainty in N_{part} and $dN/d\eta$ determination. Lines indicate the additional uncertainty due to the uncertainty in the trigger cross-section for Cu+Cu.

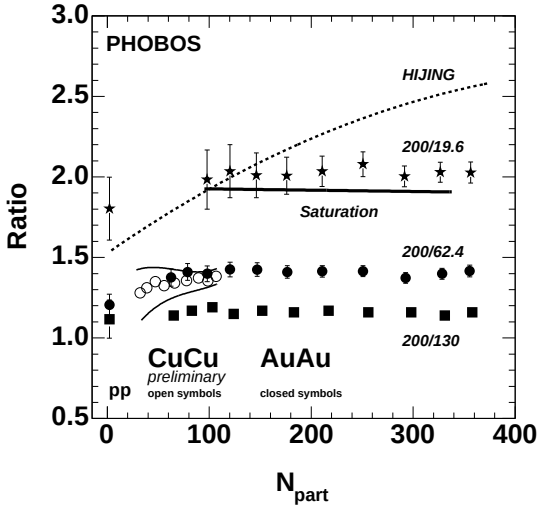

Figure 8. Ratio of mid-rapidity densities $dN/d\eta/\langle N_{part}/2\rangle$ as a function of N_{part}. Au+Au data for energies 200/19.6, 200/62.4, 200/130 (filled symbols) and Cu+Cu data for 200/62.4 (open symbols) are shown, in comparison to HIJING calculations and predictions from Kharzeev et al. for the 200/19.6 ratio [12]. Lines indicate the additional uncertainty due to the uncertainty in the trigger cross-section for Cu+Cu. Ratios for p+p collisions are shown at $N_{part} = 2$.

served increase in particle production per participant with increasing N_{part} (see Fig.7) is independent of collision energy over the full energy range of RHIC from 20 to 200 GeV.

This is illustrated in Fig.8, where we show the ratio of mid-rapidity densities as a function of N_{part} relative to 200 GeV data. All ratios, from 200/130 GeV to 200/19.6 GeV, are flat within the experimental uncertainty. This factorization of energy and centrality dependence is strongly violated in models that describe overall particle production as a superposition of independent "soft" contributions scaling like N_{part} and "hard" contributions scaling like N_{coll}, where the increase in the hard contributions is given by the increasing mini-jet production with energy. As a quantitative example, Fig. 8 shows the prediction from HIJING. It is interesting to note that the observed factorization is described in approaches based on the ideas of parton saturation [12,13].

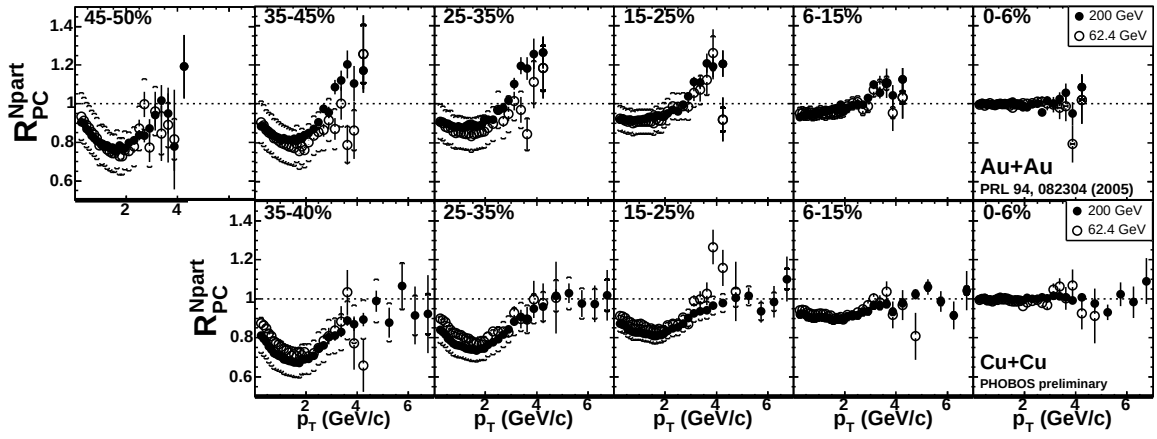

Figure 9. Ratios of yields per participant vs p_T (near mid-rapidity), relative to central collisions for bins of fractional cross-section. Central events are shown in the right-most panel. Solid symbols show 200 GeV data, open symbols show 62.4 GeV data. Top row shows Au+Au data, lower row shows Cu+Cu data. Systematic uncertainties (90% C.L.) are shown by brackets.

3.2.1. Energy and centrality factorization of p_T distributions

In an earlier publication [14], we showed that the factorization described above not only holds for the p_T-integrated yields at mid-rapidity, but also differentially over a large range of transverse momenta. This is illustrated in the top row of Fig. 9 for Au+Au collisions at 62.4 and 200 GeV. There, the quantity $R_{PC}^{N_{part}}(p_T)$, defined as

$$R_{PC}^{N_{part}}(p_T) = \frac{\langle N_{part}^{0-6\%} \rangle}{\langle N_{part} \rangle} \frac{d^2N_{AA}/dp_T d\eta}{d^2N_{AA}^{0-6\%}/dp_T d\eta}, \tag{2}$$

is shown as a function of p_T for the six centrality bins. Remarkably, the centrality evolution of the spectral shape from central to peripheral collisions is found to agree within the experimental uncertainty between 62.4 and 200 GeV, even though R_{AA} itself shows a large variation by more than a factor of two at high p_T between the two energies. The bottom row of Fig. 9 shows that the same energy-independence of the shape evolution is seen for the much smaller Cu+Cu system, when again plotting $R_{PC}(p_T)$ in bins of fractional cross-section. This apparent dominance of collision geometry, relative to expected dynamical effects, is an important feature of the data that remains to be understood.

3.2.2. Extended longitudinal scaling

As shown in earlier publications, the energy and centrality dependence of particle production factorize not only for mid-rapidity multiplicity densities. One of the most striking scaling relationships seen in nuclear collisions at RHIC is the energy-independence of particle yields at moderate to high rapidities, when viewed in the restframe of one of the colliding nuclei. This phenomenon has also been observed in p+p and p+A collisions over a large range of energies and is commonly referred to as "limiting fragmentation". PHOBOS has extended this observation not only to $dN/d\eta$ distributions in nuclear collisions at different collision centralities [5], but also to the pseudorapidity dependence of

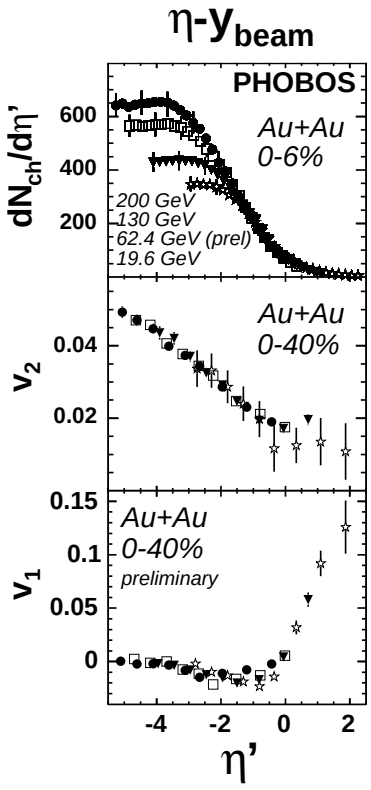

Figure 10. Dependence of $dN/d\eta'$ (top), elliptic flow v_2 (middle) and directed flow v_1 (bottom) on $\eta' = |\eta| - y_{beam}$ for Au+Au collisions at $\sqrt{s_{NN}} =$ 19.6, 62.4, 130 and 200 GeV.

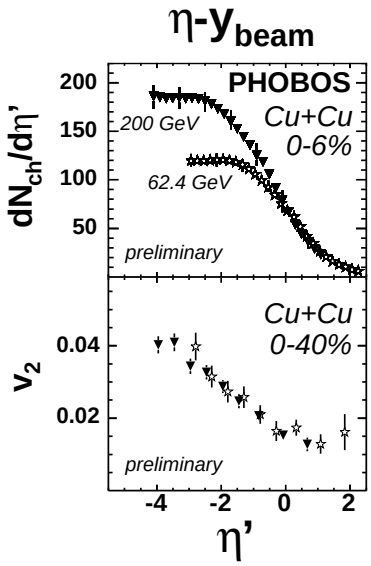

Figure 11. Dependence of $dN/d\eta'$ (top) and elliptic flow v_2 (bottom) on $\eta' = |\eta| - y_{beam}$ for Cu+Cu collisions at $\sqrt{s_{NN}} =$ 62.4 and 200 GeV (preliminary).

azimuthal anisotropies [15,16]. In Fig. 10, a compilation of results for $dN/d\eta$, the elliptic flow coefficient v_2 and the directed flow coefficient v_1 is shown for Au+Au collisions at four different collision energies from 20 to 200 GeV.

As can be seen in this figure, limiting fragmentation holds not only for the multiplicity distribution of charged hadrons, but also for observables like v_2. This is remarkable as v_2 is believed to be generated dynamically in the evolution of the collision, from presumably very different initial conditions at the different collision energies. Furthermore, Fig. 10 shows that the scaling behaviour is not confined to a small "fragmentation region" near beam-rapidity, but extends over a large part of longitudinal phase space. For this reason, we refer to this set of observations as "extended longitudinal scaling". Finally, Fig. 11 shows that the same scaling behaviour also holds for $dN/d\eta$ and v_2 in Cu+Cu. Measurements of v_1 in Cu+Cu are forthcoming.

In order to examine the connection between energy- and centrality-scaling for longitudinal distributions, it is useful to again use the ratio of yields for peripheral relative to

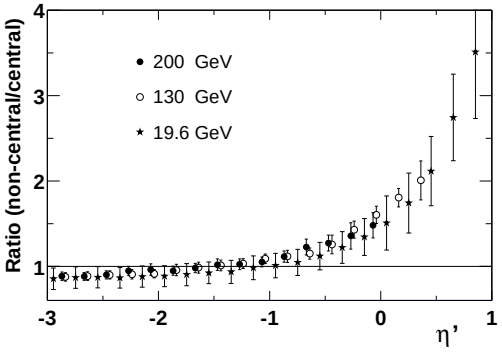

Figure 12. Ratio $R_{PC}(\eta)$ of $dN/d\eta'$ distributions for peripheral to central events for Au+Au collisions at $\sqrt{s_{NN}} =$ 19.6, 130 and 200 GeV as a function of $\eta' = |\eta| - y_{beam}$. Only systematic uncertainties (90% C.L.) are shown.

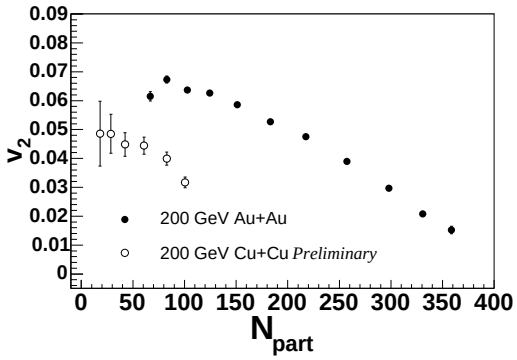

Figure 13. Average elliptic flow coefficient v_2 measured near mid-rapidity, as a function of N_{part} for Cu+Cu collisions (open symbols) and Au+Au collisions (filled symbols) at $\sqrt{s_{NN}} =$ 200 GeV. Only statistical errors are shown.

central events, $R_{PC}^{N_{part}}(\eta)$:

$$R_{PC}^{N_{part}}(\eta) = \frac{\langle N_{part}^{0-6\%} \rangle}{\langle N_{part} \rangle} \frac{dN_{AA}/d\eta}{dN_{AA}^{0-6\%}/d\eta} \tag{3}$$

In Fig. 12 we show that longitudinal distributions too, when viewed in the restframe of one of the colliding nuclei, exhibit the factorization seen for mid-rapidity yields.

In summary, the combined study of energy- and system size dependence of hadronic observables in Au+Au collisions has revealed a remarkable factorization, leading to an energy-independence of the centrality evolution for the mid-rapidity particle density, the charged hadron p_T distributions near mid-rapidity and the extended longitudinal scaling of multiplicity distributions. This factorization is particularly surprising in the context of a hard/soft picture of particle production, where the increasing mini-jet cross-sections with energy and the increasing ratio of collisions per participant, $\bar{\nu}$, couple energy and centrality dependence. It appears that the observed dominance of collision geometry, which is naturally energy-independent for a given centrality selection, is better captured in a description of the collision process based on ideas of parton saturation.

3.3. System size dependence of elliptic flow

The final question to be answered by the comparison of Au+Au and Cu+Cu data as a function of energy and centrality concerns elliptic flow, and the connection between the initial state conditions and the observed final state anisotropy. It has been argued in the past [17], that the observed flow coefficient v_2 for Au+Au closely follows the initial state eccentricity as a function of centrality. This can be seen by comparing N_{part} dependence for the Au+Au initial state eccentricity from a Glauber calculation shown in Fig. 2 and the Au+Au v_2 coefficient at mid-rapidity shown in Fig. 13. However, doubt on this crucial connection is cast by comparing the Cu+Cu calculation and data in the same figures.

Whereas the average eccentricity for Cu+Cu tends to zero for the most central collisions, the corresponding v_2 values for Cu+Cu only drop to a value of $v_2 \approx 0.03$ even for the most central collisions. This would lead to the paradoxical conclusion that for the same N_{part} and therefore the same initial area density of produced particles, the Cu+Cu system is much more effective in translating an initial eccentricity into a final state anisotropy than the Au+Au system. Alternatively, large non-flow effects mimicking a dynamically generated anisotropy could be postulated for the Cu+Cu system.

However, a possible explanation unifying the observations in Au+Au and Cu+Cu can be found by examining the underlying definition of the initial state eccentricity. This eccentricity, called ϵ_{std} in the following, is commonly defined as the average eccentricity of the distribution of participating nucleons, relative to the known reaction plane, obtained for a certain centrality class in a Glauber calculation. This definition suffers from two potential problems: It averages out the fluctuations from event-to-event in the actual participant distributions. Finite number fluctuations will lead to an eccentric nucleon distribution even for collisions with impact parameter $b = 0$. With the standard definition, these fluctuations will be averaged to zero for central events. Furthermore, the minor axis for the actual event-by-event participant distribution will in general not coincide with the impact parameter vector. The eccentricity calculated relative to the reaction plane will therefore underestimate the true eccentricity of the nucleon distribution. To study these deficiencies, we have defined an alternative measure of the eccentricty in each centrality bin, where we calculate the eccentricity for each Glauber event relative to the principal axes of the actual participant distribution (see [18]). By construction, this *participant eccentricity*, ϵ_{part}, will always be positive and will therefore average to a finite value even for the most central events. In addition, the smaller number of colliding nucleons, makes the difference between ϵ_{std} and ϵ_{part} particularly important for the Cu+Cu system relative to Au+Au. The result of a Glauber calculation for ϵ_{part} for Cu+Cu and Au+Au as a function of N_{part} can be seen in Fig. 14. As expected, ϵ_{part} remains finite even for the most central Cu+Cu collisions.

Using ϵ_{part}, we can now attempt to identify a common scaling behaviour of Cu+Cu and Au+Au collisions over a large range of collision energies and centralities. This is shown in Fig. 15, plotting the ratio of $\langle v_2 \rangle / \langle \epsilon_{part} \rangle$ versus the mid-rapidity area density of produced particles [19,20]. The data appear to exhibit a common scaling behavior over a large range in collision energy, suggesting that the efficiency for translating the initial state eccentricity estimated using ϵ_{part} into a final state anisotropy v_2 appears to only depend on the initial area density achieved in the collision. Clearly, it is a fascinating question for future experiments whether this curve saturates at higher densities or continues to rise.

4. FUTURE PHOBOS PHYSICS PROGRAM

The future physics program of PHOBOS will rely on the analysis of the existing datasets. The program is characterized by two major directions. We will use the unique acceptance of our mid-rapidity spectrometer to study particle production at the lowest transverse momenta accessible at RHIC, as a function of collision energy, centrality and colliding species. This includes studies of ϕ-meson production at very low p_T, which requires an analysis of the full high statistics datasets for Cu+Cu and Au+Au. The second

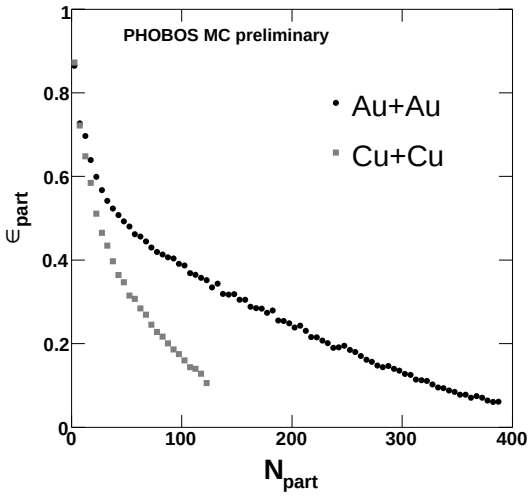

Figure 14. Participant eccentricity ϵ_{part} of the collision zone in Cu+Cu (light symbols) and Au+Au (dark symbols) as a function of N_{part} for $\sqrt{s_{NN}}$ = 200 GeV from PHOBOS Glauber MC.

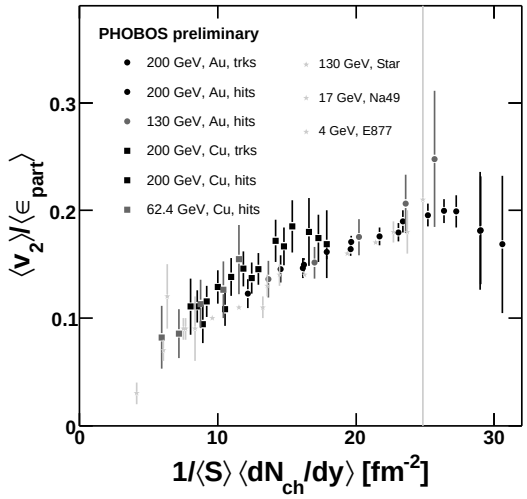

Figure 15. Ratio of v_2 coefficient to average participant eccentricity as a function of mid-rapidity area density $1/\langle S \rangle \langle dN/dy \rangle$ for Au+Au collisions at $\sqrt{s_{NN}}$ = 130 and 200 GeV and Cu+Cu collisions at $\sqrt{s_{NN}}$ = 62.4 and 200 GeV, in comparison to lower energy data from NA49 and E877.

class of studies uses the high statistics datasets in combination with the large acceptance of the multiplicity array to study fluctuations and correlations in particle production. Preliminary results from these studies are presented in separate contributions to these proceedings [21–23] and will be summarized here briefly.

4.1. Particle production at low p_T

The unique setup of the PHOBOS silicon spectrometer and its proximity to the interaction vertex allows us to detect charged particles that range out and stop in the front layers of the silicon detector. For the present analysis, we have developed an algorithm detecting particles that stop in the fifth silicon layer. Based on the total deposited energy and the specific energy loss in the silicon detectors, we can reconstruct the momentum and mass of charged particles. This allows us to measure pions, kaons and protons (summed with their anti-particles) for transverse momenta as low as 30, 90 and 140 MeV/c, respectively. For details of the reconstruction algorithm, see [24].

At this conference, new results for the centrality dependence of particle production at low p_T in Au+Au collisions at 62.4 and 200 GeV were presented, as well as results for minimum bias d+Au collisions at 200 GeV. A detailed discussion of the results can be found in [21]. As an example, Fig. 16 shows the yield for pions, kaons and protons at low p_T in combination with results at higher p_T for minimum bias d+Au collisions at 200 GeV. Both results are fully corrected, including a correction for feed-down from weak

decays. Also shown are the results of a blastwave fit to the higher p_T data, which is found to underestimate the low p_T points for d+Au, whereas for similar fits in Au+Au collisions consistency between the low and high p_T datasets is found. It is interesting to note however that the effective expansion velocity extracted from the fit to the d+Au high p_T data is $0.35c$, indicating that the physical interpretation of the extracted value has to be treated carefully.

4.2. Fluctuations and Correlations

The high statistics Au+Au dataset, in combination with the large PHOBOS acceptance, allows us to perform a search for events that in a statistically quantifiable way differ from average Au+Au events. Possible mechanisms for the occurrence of such events might be the formation of droplets due to supercooling [25] or the formation of disoriented chiral condensates [26]. While the likelihood of such scenarios is unclear, an unbiased search for "unusual" events clearly is an important part of the RHIC physics program. The details of our strategy for identifying rare events is described in [23]. Using the most central two million events of our Au+Au dataset, we determine the shape of the average uncorrected $dN/d\eta$ distribution for events in fine bins of vertex position. Similarly, the variance around the average shape in bins of η is extracted from the data. Using the average shape and variance obtained from the data, we then calculate the χ^2 of each individual event relative to the ensemble average. The resulting χ^2 distribution is shown in Fig. 17. The distribution consists of a central core close to a $\chi^2/DoF \approx 1$, with a tail out to large χ^2. In total, about 0.01% of all events are found in a region where for purely statistical fluctuations no entries would be expected. Further studies of these unusual events have shown that their rate is linearly related to the instantaneous luminosity at which the collisions were recorded. At present, we therefore have no evidence for the existence of unusual physical fluctuations. Further studies are underway to set quantitative limits on various physical scenarios.

4.3. Forward-backward multiplicity correlations

Further examination of Fig. 17 shows that the width of the χ^2 distribution around unity is significantly larger than expected for a purely Poissonian production and detection of charged particles. Thus particles appear to be produced in a correlated fashion, rather than one-by-one. This can be studied quantitatively using correlations of multiplicities in non-overlapping bins of pseudorapidity. We have performed such studies for symmetric pairs of pseudorapidity bins centered at values between $0.25 < \eta < 2.75$, varying the bin width from $0.5 < \Delta\eta < 2.0$. To quantify the relative fluctuations between the multiplicties N_F in the forward ($\eta > 0$) and N_B in the backward ($\eta < 0$) bins, we define the event-wise observable $C = (N_F - N_B)/\sqrt{N_F + N_B}$. This variable has the useful property that its variance σ_C^2 is one for independent particle emission, even when averaged over events from centrality bins of finite widths. After correction for detector and acceptance effects, which are described in [27,22], σ_C^2 can be used to study short range correlations in particle production. If particles are produced as clusters which decay with a rapidity width smaller than the typical bin width chosen in the analysis, then σ_C^2 in the absence of other correlations will directly correspond to the cluster size k, i.e. the multiplicity of decay products from each cluster. In Figs. 18 and 19, we show the dependence of σ_C^2 on the position and width of the bins used in our analysis for central

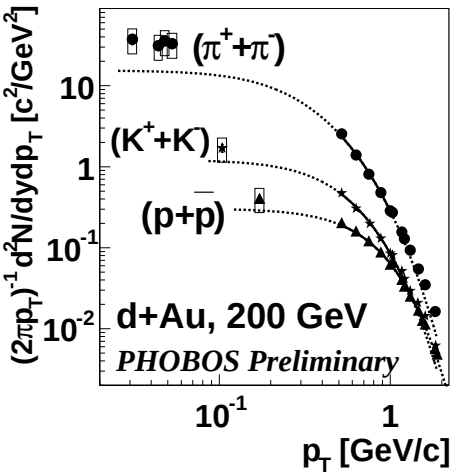

Figure 16. Transverse momentum spectra for pions, kaons and protons in 200 GeV min-bias d+Au collisions. Lines indicate the results of a blast-wave fit for data above $p_T = 0.25$ GeV/c.

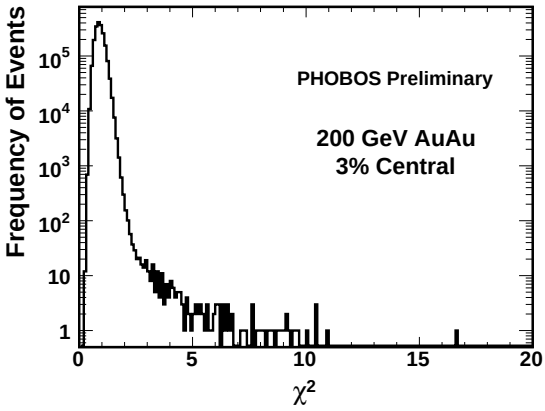

Figure 17. Reduced χ^2 distribution for event-by-event comparison of central Au+Au collisions at 200 GeV to ensemble average.

Au+Au events. The main result is that σ_C^2 is much larger than unity, in particular for larger $\Delta\eta$, indicating that particles in Au+Au collisions are not produced independently, but rather in clusters. The results are reminiscent of those obtained in similar analyses for $p + \bar{p}$ collisions [28]. The similarity of the results in A+A and $p + \bar{p}$ collisions, as well as the weak energy dependence seen in $p+\bar{p}$, could indicate that the cluster formation is a phenomenon related to common features at hadronization. This will be further tested by future studies of multiplicity correlations in Au+Au and Cu+Cu collisions as a function of collision energy. For further discussion and a comparison of the present results with event generators, see [22].

5. SUMMARY

In this paper, we have presented new results from the recent Cu+Cu run at RHIC. The data show that particle production per participant nucleon is very similar in Cu+Cu and Au+Au collisions, if one selects collisions with equivalent number of participants. This is true not only for the mid-rapidity particle density, but also for p_T spectra and the shape of the pseudorapidity distributions. Like Au+Au collisions at RHIC, the Cu+Cu data also exhibit several intriguing scaling relationships, including the extended longitudinal scaling of pseudorapidity distributions and elliptic flow, and the factorization of energy and centrality dependence. The first data on elliptic flow in Cu+Cu reveal a shape of $v_2(\eta)$ that is similar to observations in Au+Au, with a surprisingly large magnitude of v_2 near mid-rapidity relative to the expected average initial state anisotropy. We have argued that the result can be quantitavily understood, when taking fluctuations in the initial state transverse geometry into account. This leads to a universal scaling of v_2 relative to

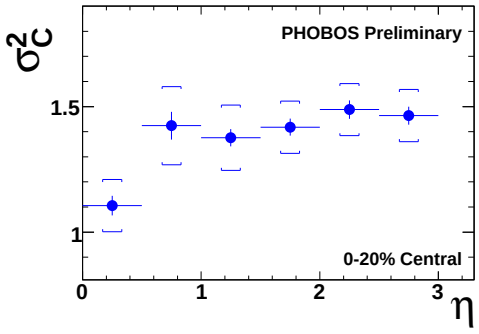

Figure 18. Dependence of the fluctuation measure σ^2_C on the position η for $\Delta\eta = 0.5$ of the forward and backward multiplicity bins for central Au+Au collisions at 200 GeV (preliminary). Systematic uncertainties (90% C.L.) are shown as brackets.

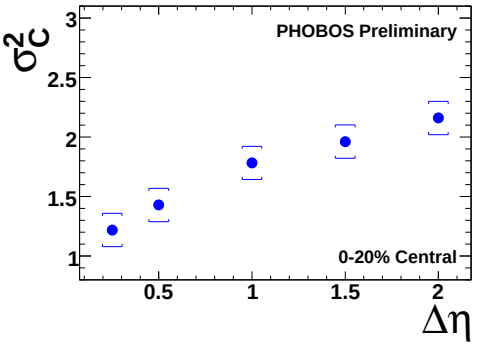

Figure 19. Dependence of the fluctuation measure σ^2_C on the width $\Delta\eta$ for $\eta = 2.0$ of the forward and backward multiplicity bins for central Au+Au collisions at 200 GeV (preliminary). Systematic uncertainties (90% C.L.) are shown as brackets.

the properly defined "participant eccentricity" in Cu+Cu and Au+Au data over a large range in collision energy. We also presented examples of the ongoing systematic study of particle production at very low transverse momenta. For Au+Au, the low p_T data agree well with extrapolations from higher p_T assuming a radially expanding source. We expect further insight into the underlying mechanisms of particle production from measurements of event-by-event fluctuations. Results were shown that revealed significant, cluster-like, correlations in final state multiplicity production, but no indication for the presence of unusual, large scale fluctuations. Overall, our data point to the importance of understanding the dynamics of the very early stage of the collision, where the scaling features observed in the final state hadron production and anisoptropies are established.

REFERENCES

1. B. B. Back *et al.*, Nucl. Phys. A **757**, 28 (2005).
2. B. B. Back *et al.* (PHOBOS Collaboration), Nucl. Instrum. Meth. A **499**, 603 (2003).
3. R. Brun and F. Rademakers, Nucl. Instrum. Meth. A **389** (1997) 81.
4. M. Ballintijn, G. Roland, R. Brun and F. Rademakers, eConf **C0303241**, TUCT004 (2003) (arXiv:physics/0306110).
5. B. B. Back *et al.* (PHOBOS Collaboration), Phys. Rev. Lett. **91**, 052303 (2003)
6. B. B. Back *et al.* (PHOBOS Collaboration), (arXiv:nucl-ex/0509034).
7. B. B. Back *et al.* (PHOBOS Collaboration), Phys. Rev. C **72**, 031901 (2005).
8. M. Gyulassy and X. N. Wang, Comput. Phys. Commun. **83**, 307 (1994).
9. B. B. Back *et al.* (PHOBOS Collaboration), Phys. Lett. B **578**, 297 (2004).
10. S. S. Adler *et al.* (PHENIX Collaboration), Phys. Rev. C **69**, 034910 (2004).
11. B. B. Back *et al.* (PHOBOS Collaboration), Phys. Rev. C **70**, 021902 (2004).
12. D. Kharzeev, E. Levin and M. Nardi, Phys. Rev. C **71**, 054903 (2005).

13. N. Armesto, C. A. Salgado and U. A. Wiedemann, Phys. Rev. Lett. **94**, 022002 (2005).
14. B. B. Back *et al.* (PHOBOS Collaboration), Phys. Rev. Lett. **94**, 082304 (2005).
15. B. B. Back *et al.* (PHOBOS Collaboration), Phys. Rev. Lett. **94**, 122303 (2005).
16. M. Belt Tonjes *et al.* (PHOBOS Collaboration), J. Phys. G **30**, S1243 (2004).
17. K. H. Ackermann *et al.* (STAR Collaboration), Phys. Rev. Lett. **86**, 402 (2001)
18. S. Manly *et al.* (PHOBOS collaboration), these Proceedings.
19. S. A. Voloshin and A. M. Poskanzer, Phys. Lett. B **474**, 27 (2000).
20. H. Heiselberg and A. M. Levy, Phys. Rev. C **59**, 2716 (1999)
21. A. Trzupek *et al.* (PHOBOS collaboration), these Proceedings.
22. P. Steinberg *et al.* (PHOBOS collaboration), these Proceedings.
23. G. Stephans *et al.* (PHOBOS collaboration), these Proceedings.
24. B. B. Back *et al.* (PHOBOS Collaboration), Phys. Rev. C **70**, 051901 (2004).
25. I. N. Mishustin, Phys. Rev. Lett. **82**, 4779 (1999).
26. K. Rajagopal and F. Wilczek, Nucl. Phys. B **399**, 395 (1993).
27. Z. Chai *et al.* (PHOBOS Collaboration), arXiv:nucl-ex/0509027.
28. K. Alpgard *et al.* (UA5 Collaboration), Phys. Lett. B **123**, 361 (1983).